PERIODIC CONTROL OF TURBULENT BOUNDARY LAYERS

Final Report
AFOSR GRANT # FA9550-06-1-0355

Jason L. Speyer and John Kim
Mechanical and Aerospace Engineering Department
University of California, Los Angeles
Los Angeles, CA 90095-1597

March 3, 2009

Summary

Over the last two and a half years, control strategies were developed to reduce viscous drag in turbulent boundary layers, in particular, by expanding on the recent discovery that simple two-dimensional, streamwise sinusoidal waves traveling upstream sustain a channel flow with sub-laminar drag. This simple open-loop control of wall-bounded blowing and suction modifies the Reynolds shear stress distribution to directly reduce drag. This reduction is predicted by linear theory and has been confirmed with nonlinear direct numerical simulations (DNS). However, the traveling waves also induce instabilities in the channel flow. Channel flow dynamical equations linearized about a periodic flow induced by the traveling wave shows unstable modes. For small amplitude traveling waves, the linearized dynamics are fairly accurate in predicting the instabilities. Significant progress has been made in understanding the instability of the flow field induced by the upstream traveling wave using Floquet analysis, developing an appropriate linearized dynamical system for which the control design is based, and the implementation of these controllers to suppress these secondary instabilities for small amplitude traveling waves. Although the linearized dynamics are periodic in a fixed or laboratory coordinate frame, the system dynamics are time-invariant in a coordinate frame moving with the traveling wave. This allowed an enormous simplification of the controller syntheses and based on the moving coordinate frame, linear quadratic regulators (LQR) are shown to suppress these secondary instabilities. Currently, the linear models and the feedback controls designed on them are limited to somewhat small amplitude traveling waves. Since even for small amplitude traveling waves, the coupling induced by the traveling wave between wave number pairs creates a very large dynamical system. An approach to model reduction, which might have enormous benefit in constructing reduced models for large amplitude traveling waves for control design, has also been developed during this grant period.

AFRL-SR-AR-TR-09-0147

REPORT DOCUMENTATION PAGE

PLEASE DO NOT RETURN YOUR FORM TO THE ABOVE ORGANIZATION.

1. REPORT DATE *(DD-MM-YYYY)*	2. REPORT TYPE	3. DATES COVERED *(From - To)*
03-03-2009	Final Technical	15 May 2006 - 30 Nov 2008

4. TITLE AND SUBTITLE
PERIODIC CONTROL OF TURBULENT BOUNDARY LAYERS

5a. CONTRACT NUMBER
FA9550-06-1-0355

5b. GRANT NUMBER

5c. PROGRAM ELEMENT NUMBER

6. AUTHOR(S)
Jason Speyer, John Kim

5d. PROJECT NUMBER

5e. TASK NUMBER

5f. WORK UNIT NUMBER

7. PERFORMING ORGANIZATION NAME(S) AND ADDRESS(ES)
Mechanical and Aerospace Engineering Department
University of California, Los Angeles
Los Angeles, CA 90095-1597

8. PERFORMING ORGANIZATION REPORT NUMBER

9. SPONSORING/MONITORING AGENCY NAME(S) AND ADDRESS(ES)
Air Force Office of Scientific Research
875 N. Randolph St
Arlington, VA 22203

10. SPONSOR/MONITOR'S ACRONYM(S)
AFOSR

11. SPONSOR/MONITOR'S REPORT NUMBER(S)
FA9550-06-1-0355

12. DISTRIBUTION/AVAILABILITY STATEMENT
Distribution A

13. SUPPLEMENTARY NOTES

14. ABSTRACT

15. SUBJECT TERMS

16. SECURITY CLASSIFICATION OF:			17. LIMITATION OF ABSTRACT	18. NUMBER OF PAGES	19a. NAME OF RESPONSIBLE PERSON
a. REPORT	b. ABSTRACT	c. THIS PAGE			19b. TELEPHONE NUMBER *(Include area code)*
U	U	U	UU	17	

Contents

1 Introduction

The ability to control flows, turbulent flows in particular, has great consequences in many science and engineering applications. Successful flow control can lead to, among other things, reduced drag and increased lift. Agility and maneuverability for military aircraft and weapons can be significantly improved through flow control. Successful flow control requires a thorough understanding of the underlying physics of the flow under control, efficient control algorithms, and robust sensors and actuators, all of which have been less than satisfactory despite the great interest they have garnered over the years. Great strides have been made recently through advancements in computational fluid dynamics, control theories, and micro- and nano-fabrication technology. A better understanding of the role of organized structures observed in boundary layers has led to new approaches of controlling theses flows, while a better understanding of the instability of free-shear flows has resulted in large control effects with minimal control input. The ability to manufacture a large number of sensors and actuators that are capable of sensing and actuating small scales in turbulent flows, for example, affords a new opportunity for turbulence control, which has previously proven to be difficult due, in part, to the inability to control small-scale motions (on the order of a micro meter, for example, for commercial airplanes). Modern systems theoretic approach to flow control, particularly turbulence control, which has been hindered by the fact that fluid flows are nonlinear and high-dimensional systems, provides new possibilities and challenges for flow control. In contrast to traditional approaches, in which control input is designed on a trial-and-error basis and/or based on the control designer's physical insight into the flow, the systems theoretic approach uses the dynamical equations to formulate controls to meet a specified objective. In our studies [1–5], we have successfully applied systems theoretic approaches to design optimal controllers that substantially reduced drag with wall blowing/suction along the channel wall.

These controllers are all derived by applying modern control synthesis techniques to the spectral decomposition of the Navier-Stokes equations, linearized for small perturbations around the Poiseuille mean profile. This discretization decouples the dynamics to independent sub-systems by discretization spatial wavenumbers. This allows an immediate reduction in control size by simply applying controllers to certain sub-systems [3]. Even lacking the nonlinear terms of the channel flow, these controls have reduced the viscous drag by 15% to 18% [4]. The controls also lack a direct measure for drag reduction, for example, in [4] the control aims to reduce the quadratic of the wall-shear stress fluctuations. Other indirect cost criteria result in approximately the same drag reduction performance [5].

In an effort to move past this apparent performance limit, we began to explore open-loop periodic controls, to take advantage of transient drag reduction found in almost all of the feedback controllers. During these numerical experiments, we discovered that a simple, sinusoidal wave of wall-normal blowing and suction at the walls could not only drive down but sustain drag reduction in the channel (See Appendix A). In fact, in DNS initialized with a laminar flow field, the upstream traveling wave sustained a flow field with sub-laminar drag characteristics. Furthermore, we found that the linear models used in our feedback control synthesis were sufficient to charac-

terize the relationship of the traveling wave parameters (its speed, direction, amplitude, and spatial wavenumber) to the drag reduction that can be achieved.

While certainly computationally more efficient than DNS, the linear drag reduction prediction becomes less accurate with larger amplitude waves; this is reasonable since larger amplitudes waves will induce larger amplitude velocities, which then violate the small perturbation assumption of the linear model. The linear model also suffers from other limitations. It can only predict the sub-laminar drag steady-state flow that is found when the DNS is initialized with a purely laminar flow field. With an initially self-sustaining turbulent flow field or a laminar flow field with perturbations, the channel flow settles to a different, turbulent equilibrium than the laminar one. The linear model cannot predict the turbulent equilibrium, since that equilibrium is most probably sustained by nonlinear effects. However, it is troubling that the linear model cannot predict any instabilities to explain the transition from laminar to turbulent equilibria.

As a first step to more accurately characterize the traveling wave induced flow field, Floquet analysis is used to derive the dynamics of the perturbations about the *periodic* base flow (See [6, Appendix A]). Specifically, the perturbations are characterized as having the spatial and temporal periodicity of the traveling wave. Then, the invariant portion of the dynamics models the stability characteristics of the traveling wave induced flow. Using a 2D Fourier decomposition in the streamwise and spanwise directions, the base flow is thus represented as a linear super-position of the Poiseuille mean profile as well as velocities (along the entire channel height not just at the wall) at the wavenumber of the traveling wave. The governing equations are now coupled among perturbations at different wavenumbers. This is in contrast to the linear models previously used, which are decoupled by wavenumber. While requiring larger system sizes, this linear model does clearly show that the traveling wave induces secondary instabilities in the channel, particularly in three-dimensional perturbation wavenumbers.

While the Floquet analysis provides a linear method by which to characterize the stability of the traveling induced velocity, it does not directly provide system equations appropriate for control synthesis. Primarily, it ties both the spatial and temporal periodicity to the traveling wave. The spectral decomposition method used in our previous studies results in a time-varying system matrices when applied to the traveling wave induced flow. Due to the size of the coupled dynamics, it is prohibitively expensive to calculate the transition matrix to properly identify the temporal periodic and time-invariant behavior. However, by discretizing the traveling wave induced channel flow in a frame of reference moving with the traveling wave, *linear time-invariant (LTI) system* equations appropriate for control synthesis can be derived. The moving frame isolates only the temporal periodicity of the flow. The stability of these linear models match those of the Floquet analysis and similarly couple the perturbation at different wavenumbers. For low amplitude traveling waves, we have successfully designed and applied linear quadratic regulators (LQR) to suppress the growing perturbation energy of the induced instabilities (see Section 4).

Our study so far demonstrates that for small amplitudes of the traveling wave, we can accurately analyze and design feedback controls for transition suppression using linear system theoretic

methods. It is clear that higher amplitude traveling waves produces dramatic drag reduction. However, this comes at the cost of requiring more power to implement the traveling wave and results in less efficient controllers than other strategies using the same actuation [6, Appendix A]. Furthermore, we have observed that even with high amplitudes, the traveling wave settles the channel flow to two different equilibrium depending on the initial flow state, i.e. turbulent or laminar. Since high amplitude traveling waves have such profound effect, further analysis of these flow fields may yield optimal feedback controls that can drive the channel flow from the steady-state turbulent flow to the sustained sub-laminar drag, or laminar, flows. This would allow the use of lower amplitude traveling waves (with their lower power requirements) to achieve sub-laminar flows even when starting from a turbulent flow field. Such a system of traveling wave and feedback control would represent a highly efficient drag reduction control.

In the following sections, we provide further details of the work done in our studies. The observed behavior of upstream traveling waves (particularly in terms of its drag reduction capability) is described in Section 2, the linear models that have been derived for analyzing the stability characteristics of the traveling wave induced flow field are presented in Section 3, the controls derived and applied to suppress transition to a turbulent steady-state flow are given in Section 4, and an approach to model reduction for nonlinear systems is considered in Section 5.

2 Upstream Traveling Wave: sub-laminar drag

Two-dimensional streamwise waves of wall-bounded, wall-normal blowing and suction made to travel *upstream* can reduce skin-friction drag substantially. As can be seen in Figure 1, the effect on drag reduction is quite dramatic for large amplitudes of the traveling wave. For this simple, open-loop control, wall-normal velocities are introduced at the upper and lower walls:

$$\begin{aligned} v_{\text{upper}}(x,t) &= -a\,\cos\bigl(k_x(x-ct)\bigr) \quad \text{and} \\ v_{\text{lower}}(x,t) &= a\,\cos\bigl(k_x(x-ct)\bigr) \quad , \end{aligned} \tag{1}$$

where a is a scalar, c is the wave speed normalized to the mean centerline velocity, and k_x is the streamwise wavenumber. The blowing and suction are applied on the upper and lower walls in varicose mode, where suction (and blowing) occurs at the same streamwise location at both walls. By convention, the control on the upper wall has a minus sign to denote blowing (positive sign for suction) and the opposite for the lower wall.

The upstream traveling waves sustains drag reduction by forcing a distribution of the Reynolds shear stress favorable for drag reduction. The Fukagata *et al.* [7, 8] elucidates the drag reduction mechanism by relating the skin-friction drag in a fully developed channel flow to the Reynolds shear stress:

$$\langle D\rangle_\infty = \langle D\rangle_\ell + \frac{3\mathrm{Re}}{2}\int_{-1}^{1} \overline{u\,v}\; y\; dy\;, \tag{2}$$

where $\langle D \rangle_\infty$ represents the total skin-friction drag, $\langle D \rangle_\ell$ denotes the laminar drag value, Re is the Reynolds number of flow centerline velocity, u is the streamwise perturbation velocity, v is the wall-normal perturbation velocity, $\overline{u\,v}$ denotes the Reynolds shear stress, and y denotes the wall-normal direction. The traveling waves drive the integral of the Reynolds shear stress to become negative near the upper wall (positive near the lower wall) by inducing u to be phase shifted from v in the direction of the traveling wave. This phase shift makes $\overline{u\,v}$ negative with upstream traveling wave, which in turn induced net mass flux in the opposite direction. This translates to smaller pressure gradient to drive the same net mass flux or more mass flux for the same channel pressure gradient, which, in a channel flow, translate to less viscous drag. The negative contribution of the Reynolds shear stress integral can be approximated by solving the Orr-Sommerfeld equation around the Poiseuille channel flow, subject to controls in the form of wall-bounded wall-normal velocities [6, Appendix A]:

$$\dot{\vec{x}} = \mathrm{A}\,\vec{x} + \mathrm{B}\,\vec{u} \quad , \tag{3}$$

where $\vec{x}$ represents the perturbation state, A the dynamics, B the input matrix, and $\vec{u}$ the control input (see [1–5] for details of this approach). B and $\vec{u}$ are defined to represent the effect of wall-bounded, wall-blowing suction and blowing. We can find the state $\vec{x}$, the perturbation velocities,

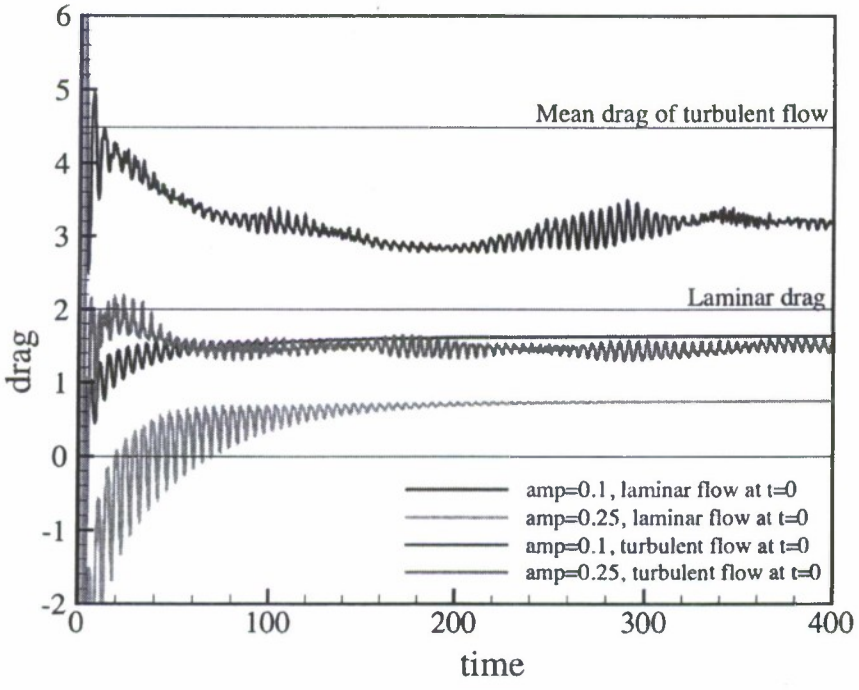

Figure 1: 3D DNS time history of drag at Re = 2000. Upstream traveling wave applied at $k_x = 0.5$, speed -2 (upstream) to initially laminar or turbulent flow.

at any time for any known control $\vec{u}$ by the solution to (3):

$$\vec{x}(t) = e^{\mathbf{A}t}\vec{x}(0) + \int_0^t e^{\mathbf{A}\tau}\mathbf{B}\vec{u}(\tau)\mathrm{d}\tau \quad . \tag{4}$$

The Reynolds shear stress integral calculated from this linear equation matches the drag reduction found in DNS.

It should also be noted that the power input requirements are also tied to the amplitude of the traveling wave. Ignoring the friction that any actuator would have to overcome, we define input power as being the work necessary to maintain the traveling wave: $P_{\text{in}} = \overline{(p_w + 0.5\, v_w^2)\, v_w}$, where p_w represents the pressure at the wall. Efficiency is defined as the ratio of the mean pressure gradient with the traveling wave (P_{wv}) plus the input power to the pressure gradient without the traveling wave (P_0) needed to maintain the same net mass flux through the channel, or

$$\eta = \frac{P_{wv} + P_{\text{in}}}{P_0} \quad .$$

For the cases shown in Figure 1, the efficiencies are 0.76 and 0.81 for the amplitude 0.1 and 0.25 cases, respectively, with associated drag reduction of 30% and 70% [6, Appendix A]. While the drag reduction is dramatic, we see that the input power requirements increase with higher amplitudes and the efficiencies are worse than other recent control strategies. For example, the opposition control of Choi *et al.* [9] has an efficiency of 70% with 30% drag reduction. With the 0.25 amplitude traveling wave, P_{wv}/P_0 is expected to be 0.3, which means P_{in}/P_0 is 0.51. This means more power is used to pump the fluid in and out of the walls than through the channel itself. Once actuation friction (of the fluid through perforated walls, for example) is taken into account, the higher amplitude traveling wave efficiencies will only get worse. It seems apparent that lower amplitude traveling waves are more desirable in terms of control efficiency.

Finally, while the linearized Navier-Stokes equations provides a computationally efficient basis for analyzing the drag reduction that traveling waves may gain, they are not particularly accurate for describing the dynamics of the traveling wave induced flow. In particular, they do show the instabilities of the traveling wave induced flow. While the different equilibria between the initially laminar and turbulent flows shown Figure 1 could be explained as nonlinear effects beyond the scope of any linear model, any growth that transitions the flow from the laminar steady-state to the turbulent steady-state should appear as a linear instability. Taking the lower amplitude case of Figure 1 as a case study, we find that starting the DNS with a slightly perturbed laminar flow results in transition to the turbulent equilibrium (see Figure 2). This transition is not observed in the DNS of Figure 1 since the initial laminar flow field did not introduce perturbations into an unstable mode; we have to wait a very long time for round-off error to eventually grow to finite amplitudes. With a small perturbation, the transition behavior can be observed sooner and points to an instability within the linear regime about the traveling wave induced base flow.

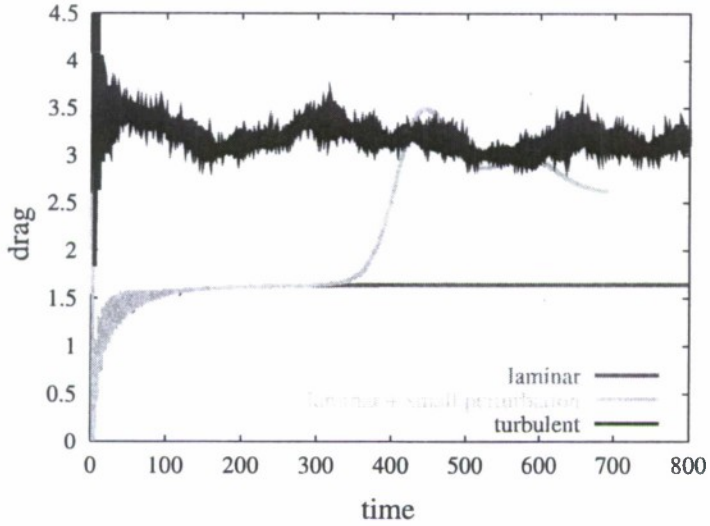

Figure 2: Re = 2000 3D DNS with traveling wave of amplitude 0.1 and upstream speed of 2 applied to laminar, laminar plus small amplitude perturbations, and fully turbulent initial flows.

3 Linear Modeling of Periodic Flow

It is clear from the results discussed in the previous section that a more accurate model of the traveling wave induced flow is needed. As a first step, we use strictly linear methods to derive such a model. Defining the control input $\vec{u}$ in equation (4) as a simple cosine function as dictated by (1), the solution to equation (4) is clearly periodic in time. So, we now assume that the base flow in the channel is described as linear super-position of the Poiseuille channel flow and the traveling wave induced velocities as found by (4):

$$\begin{aligned} u &= U + u_c + u' \quad \text{(streamwise velocity)}, \\ v &= v_c + v' \quad \text{(wall-normal velocity), and} \\ w &= w_c + w' \quad \text{(spanwise velocity).} \end{aligned}$$

The "c" subscript is introduced to indicate the velocities found by solving equation (4), i.e. the traveling wave induced velocities. Essentially, all the induced velocities are assumed to be of the following form (using wall-normal velocity as an example):

$$v_c = \hat{v}_c(y)e^{\hat{i}k_x(x-ct)} + \hat{v}_c^*(y)e^{-\hat{i}k_x(x-ct)} \quad , \tag{5}$$

where $\hat{v}_c$ is an appropriate amplitude function and and $\hat{v}_c^*$ is its complex conjugate. The mean profile, U, is still assumed to be the parabolic profile of the Poiseuille channel flow. Treating the traveling wave as a primary disturbance [10], linear dynamical equations are derived for the

perturbation velocities, u', v', and w', by using Floquet analysis in the manner described by [11, 12] (using wall-normal velocity as a sample):

$$v' = e^{(i\alpha x + i\beta z - i\omega t)} \sum_{n=-\infty}^{\infty} e^{ink_x(x-ct)} \hat{v}(y) \quad . \tag{6}$$

Here, α and β represent perturbation wavenumbers, ω the temporal growth (or decay) rate, $\hat{v}(y)$ is an appropriate amplitude function, and k_x and c are the same as in (1). The dynamical equations that result from using this decomposition are coupled between the perturbation states at different 2D Fourier wavenumbers:

$$\frac{\mathrm{d}}{\mathrm{d}t}\begin{bmatrix} \vdots \\ \vec{x}_{-1} \\ \vec{x}_0 \\ \vec{x}_1 \\ \vdots \end{bmatrix} = \overbrace{\begin{bmatrix} \ddots & & & & & \\ \mathbf{M}_{-1} & \mathbf{A}_{-1} & \mathbf{P}_{-1} & & & \\ & \mathbf{M}_0 & \mathbf{A}_0 & \mathbf{P}_0 & & \\ & & \mathbf{M}_1 & \mathbf{A}_1 & \mathbf{P}_1 & \\ & & & & & \ddots \end{bmatrix}}^{\tilde{\mathbf{A}}} \begin{bmatrix} \vdots \\ \vec{x}_{-1} \\ \vec{x}_0 \\ \vec{x}_1 \\ \vdots \end{bmatrix} \quad . \tag{7}$$

We introduce subscripts to $\vec{x}$ to indicate that they are perturbation velocities at different wavenumbers. $\mathbf{M}$, $\mathbf{A}$, and $\mathbf{P}$ are square, time-invariant matrices of appropriate size describing the coupling dynamics. This is in contrast to the linear model of the Poiseuille channel flow (3) where the perturbation states at different wavenumbers are decoupled.

As done in [11, 12], we truncate the $\tilde{\mathbf{A}}$ matrix to ± 1 wavenumbers. We find that, for small amplitude traveling waves, this completely linear approach results in a linear model that shows instabilities. For example, at Re = 5000, a wave of amplitude 0.008 (normalized to the centerline velocity of the channel) traveling upstream at a normalized speed of 2 induces an instability at the first spanwise perturbation wavenumber. As can been seen in Figure 3, this linear model accurately predicts the instability induced by the traveling wave.

4 Transition Control of Periodic Flow

The Floquet analysis linear model described in the previous section is not directly usable for control synthesis. The Floquet analysis model is primarily interested in describing the stability characteristics for any possible perturbation in the flow, while for the control synthesis, we want ordinary differential equations that model the dynamics of the entire channel. The subtle but important difference is that the latter makes no assumption of the temporal periodicity while Floquet analysis recognizes that all perturbations would share the periodicity of the primary disturbance. Of course, this will require that the computational box be of sufficient resolution to properly resolve not only the perturbation but the traveling wave and its induced velocities.

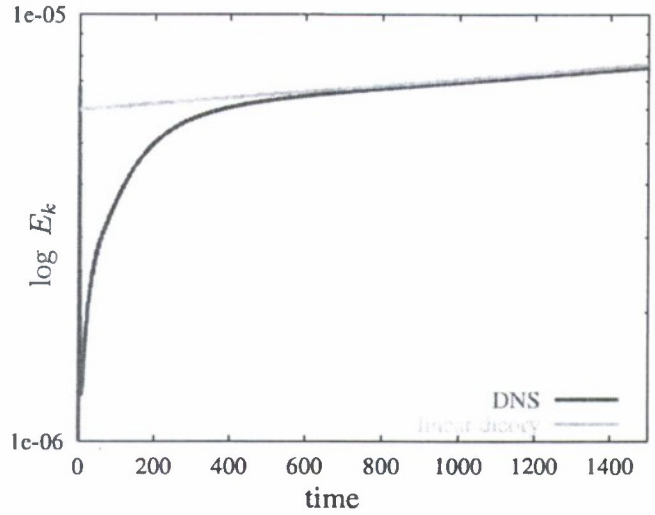

Figure 3: Plot of the log of perturbation energy at first spanwise wavenumber for flow at Re = 5000 DNS with traveling wave of amplitude 0.008 and upstream speed of 2. DNS initialized on a laminar plus small amplitude perturbation flow field.

If the decomposition method used in our previous studies (as noted in the introduction) is applied to the traveling wave induced flow dynamics, we derive a time-varying equation. In order to separate the temporal periodicity as per Floquet Theory, we would construct a transition matrix and integrate it over an assumed period. In our case, the period would be determined by the speed of the traveling wave. However, similar to the results denoted by (6) and (7), these equations are coupled for all spatial wavenumbers, thus making the computation of the transition matrix very difficult, if not prohibitively expensive.

However, the above mentioned difficulty can be avoided by considering the spatial 2D Fourier decomposition in a reference frame that moves with the traveling wave. This results in linear time-*invariant* state-space equations. We change the coordinate frame such that $t' = t$, $x' = x - ct$, $y' = y$, and $z' = z$. Note that the " $'$ " is used here to represent the moving frame in relation to the static or laboratory frame. This modifies the traveling wave definition to:

$$\begin{aligned} v_{\text{upper}}(x',t) &= -a\,\cos\big(k_x x'\big) \quad \text{and} \\ v_{\text{lower}}(x',t) &= a\,\cos\big(k_x x'\big) \quad . \end{aligned} \tag{8}$$

The 2D Fourier decomposition is now taken in the moving frame, so any perturbation velocity is defined as follows (again using the wall-normal velocity as an example):

$$v' = \sum_{\substack{n=-N,\\ m=-M}}^{N,M} \hat{v}(t',y') e^{\hat{\imath} n \alpha_0 x' + \hat{\imath} m \beta_0 z'} \quad , \tag{9}$$

where α_0 and β_0 represent the fundamental wavenumbers of the discretization and $\hat{v}(t', y')$ is, again, an appropriate amplitude function but now also a function of time. This discretization results in state-space system equations in the standard control form:

$$\dot{\bar{x}} = \overline{\mathbf{A}}\,\bar{x} + \overline{\mathbf{B}}\,\bar{u} \quad , \tag{10}$$

where $\bar{x}$ are the collection of $\vec{x}$ at different wavenumbers as in (7), $\overline{\mathbf{A}}$ is the time-invariant dynamical matrix, $\bar{u}$ is a similar collection of the $\vec{u}$ in (3), and $\overline{\mathbf{B}}$ is the time-invariant input matrix that couples the input at different wavenumbers. $\overline{\mathbf{A}}$ is quite similar to $\tilde{\mathbf{A}}$ in that it demonstrates the same stability characteristics and has a similar structure (in terms of non-zero elements). The essential difference is in terms of the temporal oscillatory characteristics in the dynamical equations. Using the notations introduced in (7), the diagonal elements of $\overline{\mathbf{A}}$, i.e. $\mathbf{A}$, are displaced by $\hat{\imath}\, n\alpha_0\, c\, \mathbf{I}$ ($\mathbf{I}$ is an identity matrix of with the dimension of $\mathbf{A}$). This shift does not effect the growth or decay rate of the perturbations. However, the LTI state-space equations (or system matrices) derived by this approach is appropriate for any systems theoretic approach.

Truncating these coupled system matrices to include 5 perturbation wavenumber states, we designed an linear quadratic regulator (LQR) to suppress the induced instabilities observed in Section 3. Based on the coupled dynamics of (10) in a moving coordinate frame, the linear-quadratic problem is to find a feedback control $\bar{u}$ that minimizes the quadratic cost

$$J^o = \min_{\bar{u}} \int_t^\infty \left(\bar{x}^T \mathbf{Q} \bar{x} + \gamma \bar{u}^T \mathbf{R} \bar{u}\right) d\tau \tag{11}$$

subject to (10). $\mathbf{Q}$ and $\mathbf{R}$ are taken as the identity and γ is used as a tuning parameter. The solution is an optimal control linearily related to the state and this controller is called the linear quadratic regulator (LQR). Note that the 3 state truncated system has the same unstable modes as the 5 state models. The 5 state models are used as an initial starting point. It may be possible to design an effective controller using the 3 state linear models. As a preliminary step, for flow at Re = 5000 DNS with traveling wave of amplitude 0.008 and upstream speed of 2, we calculated the feedback control for the 5 state models. The feedback controller required the solution to the algebraic Riccati equation based on the coupled the 5 state model and successfully suppress the instability in DNS (see Figure 4). While the result is dramatic in terms of perturbation energy growth, the solution to the algebraic Riccati equation (ARE) in the LQR synthesis is now about 12 times larger than in our previous studies (based on the 5 state model). It should be noted that the feedback control gains found here is periodic in time since the discretization is performed in a moving frame of reference. Perturbations and control inputs that are not periodic in the moving frame of reference become periodic in the static frame of reference. So while classic LTI control synthesis techniques are being used, it is important to keep in mind that the dynamical system, coefficients, and control gains are, in fact, periodic in the .

Experiments where made to significantly increase the amplitude of the traveling wave and we succeeded after some time to control the stronger secondary instabilities induced by the traveling wave. For the flow at Re = 5000 with a traveling wave of amp = 0.03 c = -2 at (0.5,0), we have

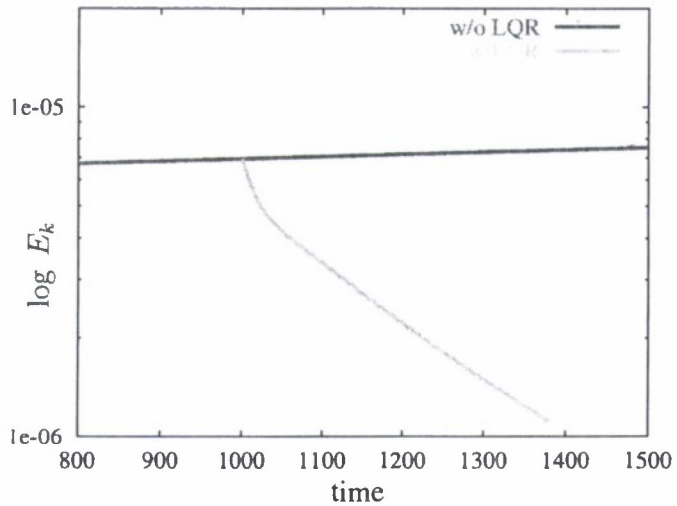

Figure 4: Plot of the log of perturbation energy at the first spanwise wavenumber for flow at Re = 5000 DNS with traveling wave of amplitude 0.008 and upstream speed of 2, with and without LQR.

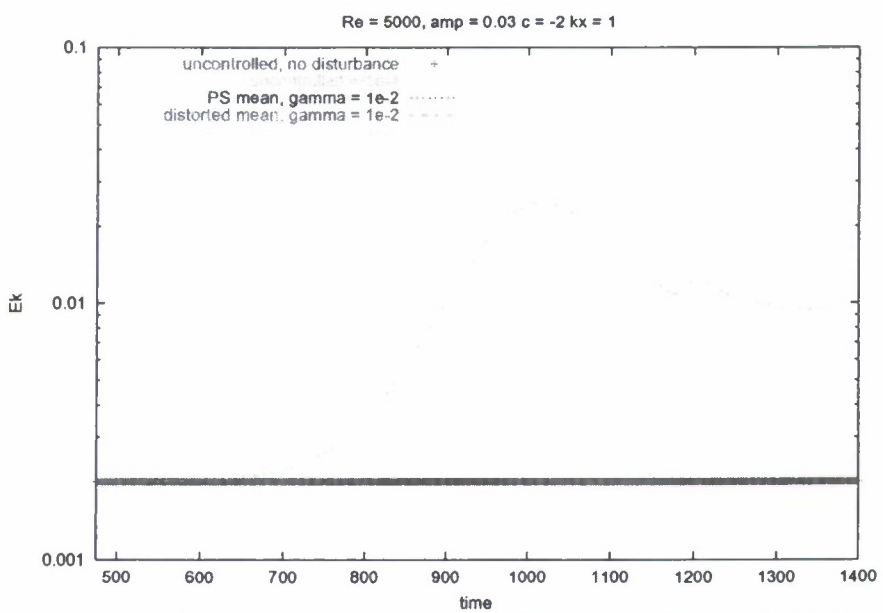

Figure 5: Plot of the log of total perturbation energy for flow at Re = 5000 DNS with traveling wave of amplitude 0.03 and upstream speed of 2, with and without LQR.

seen instabilities induced in the linear, coupled-state system for the *first 6 spanwise wavenumbers*. Initializing the DNS with a Poiseuille flow with randomized perturbations of amplitude 1e-4

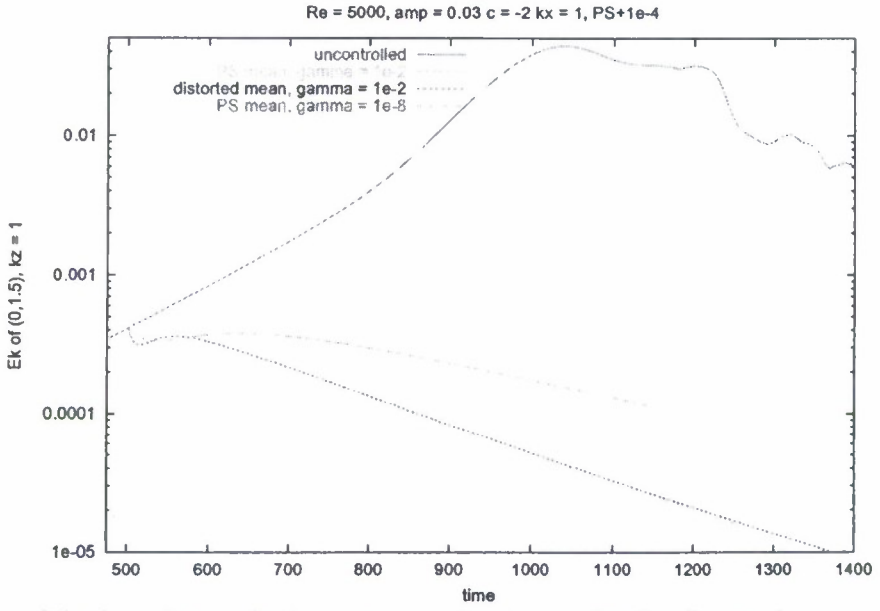

Figure 6: Plot of the log of perturbation energy at the $k_z = 1$ for the distorted mean and Poiseuille mean at Re = 5000 DNS with traveling wave of amplitude 0.03 and upstream speed of 2, with and without LQR.

demonstrates this instabilities quite nicely, see Figure 5. Three aspects of the higher amplitude traveling wave are increase value of the instabilities, the number of spanwise wavenumbers that the instabilities appear, and the number of instabilities in at each spanwise wavenumber. For the traveling wave of amplitude .03 the first six spanwise wavenumbers had secondary instabilities. For each spanwise wavenumber it was assumed that the coupled system matrices were truncated to include 5 perturbation spanwise wavenumber states. The controller are "turned on" at t =500. The results are shown in Figures 5-11 for all the controllers working together (Figure 5) and then showing the effect of each spanwise LQR controller on damping the secondary instabilities for spanwise wavenumbers k_1 to k_6 (Figures 6-11). Each plot is given as the log of energy verses time. In each Figure we compare different weighting values of γ and linear models based on either the steady-state 2D (distorted) mean profile or the Poiseuille mean profile. Plotted in Figure 5 is the log of total perturbation energy for controlled flow using LQR for various values of γ in the quadratic cost criterion. The controlled flow are all found in the red strip where the energy of the traveling wave dominates. As can be seen in Figures 6-11 the LQG controller damps out the secondary instabilities dramatically.

While the numerical sizes at these low Reynolds numbers remain manageable, the size of the controller will need to be carefully considered in any continuing proposed study that attempts to suppress larger secondary instabilities generated from larger amplitude traveling waves.

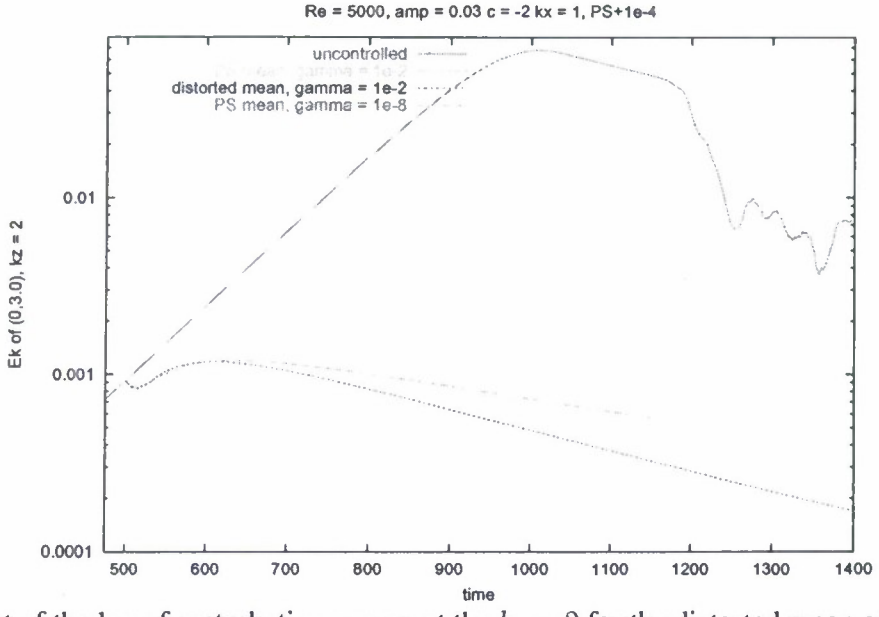

Figure 7: Plot of the log of perturbation energy at the $k_z = 2$ for the distorted mean and Poiseuille mean at Re = 5000 DNS with traveling wave of amplitude 0.03 and upstream speed of 2, with and without LQR.

5 Model Reduction

The linear models to represent the traveling wave induced channel flow are seen to be quite large and will increase with the traveling wave amplitude. In comparison to the channel flow equations in our previous studies, these models will be a minimum three or more times larger. It will become imperative that these linear models be reduced if they are to applied as real-time feedback controllers. An additional criteria for model reduction that can be added relatively easily is observability. In order to define observability, we would need to define a measurement equation to the dynamical equation, i.e. (10) as an example:

$$\begin{aligned} \dot{\bar{x}} &= \overline{\mathbf{A}}\,\bar{x} + \overline{\mathbf{B}}\,\bar{u} \\ \bar{z} &= \overline{\mathbf{C}}\,\bar{x} + \overline{\mathbf{D}}\,\bar{u} \quad , \end{aligned} \tag{12}$$

where $\bar{z}$ represents the measurement. $\overline{\mathbf{C}}$ is the state measurement matrix, and $\overline{\mathbf{D}}$ is referred to as the feedthrough term[1].

In our previous studies, we have already developed a method to make use of controllability and observability to reduce the model size, as alluded to in the previous section and shown in [13, Appendix C]. The method is finds a balanced realization on a mode by mode basis, by calculating

[1]Depending on the measurement and spectral approximation, there may be no feedthrough term [see Appendix D]

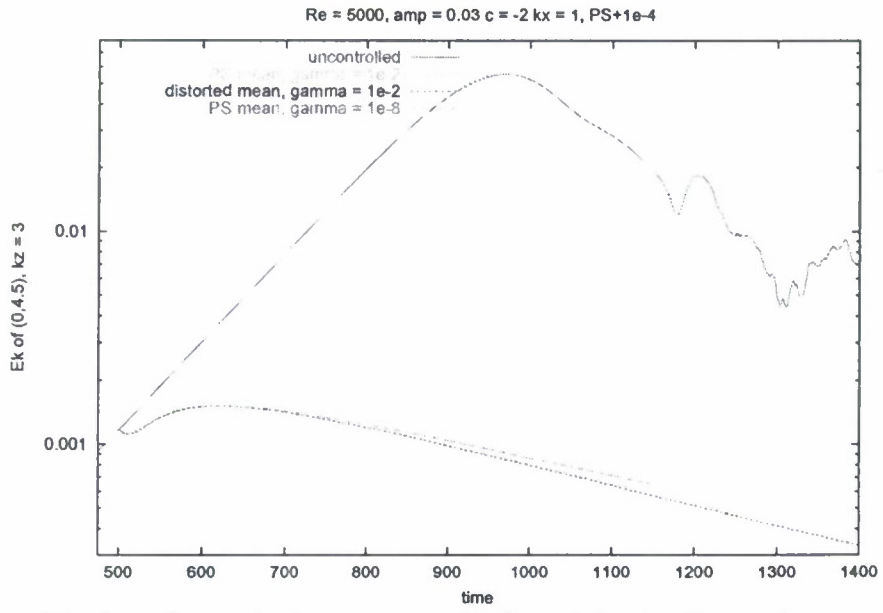

Figure 8: Plot of the log of perturbation energy at the $k_z = 3$ for the distorted mean and Poiseuille mean at Re = 5000 DNS with traveling wave of amplitude 0.03 and upstream speed of 2, with and without LQR.

the modal controllability and observability gramians [3]. It remains to be seen if the approach will work with the traveling wave induced channel flow models. Their sheer size will pose some numerical challenges.

Given the limitations of a linear model to approximate nonlinear flows, system identification techniques that do identify nonlinear input/output systems are important. These techniques use empirical measurements to directly derive models, preferably, of sizes smaller than the computational box size of the DNS. One such approach is to use snapshots of the traveling wave induced turbulent flow to construct a reduced-order model by a generalized balanced proper orthogonal decomposition (POD) scheme [13, Appendix C]. A linear model was constructed first and is presented in [13, Appendix C], but nonlinear models have also been considered, where preliminary findings indicate good matching of the reduced-order nonlinear system with the original nonlinear system. The essential nonlinear dynamics of the reduced-order nonlinear system are used to guide the controller design. The only draw back to these methods is that the dynamical equations derived are something of a black box, having compromised physical intuition, and these approximation models will vary depending on sampling and *a priori* assumed sizes. Furthermore, DNS simulations would need to be run in order to collect the data needed to obtain the models.

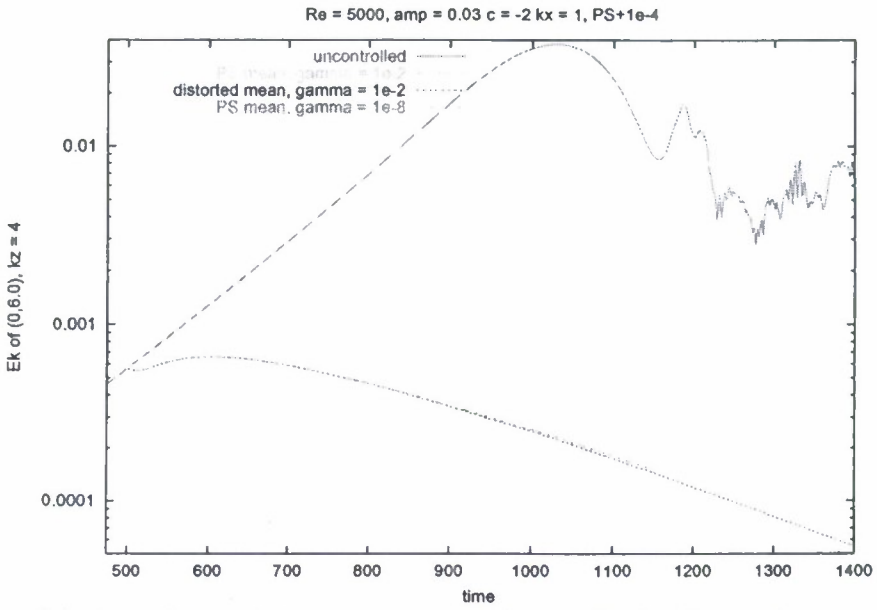

Figure 9: Plot of the log of perturbation energy at the $k_z = 4$ for the distorted mean and Poiseuille mean at $\mathrm{Re} = 5000$ DNS with traveling wave of amplitude 0.03 and upstream speed of 2, with and without LQR.

6 Conclusions

In our previous study, we used the three-dimensional Navier-Stokes equations linearized about the Poiseuille channel flow as the basis for designing reduced-order controllers. In this study these same linear models are sufficient to demonstrate the efficacy of traveling waves, particularly upstream traveling waves, of wall-bounded, wall-normal blowing and suction to effect mean properties of the flow, such as viscous drag. However, they are insufficient to fully characterize the traveling wave induced flow, particularly in terms of stability. Floquet analysis of the perturbations around the traveling wave induced flow leads to dynamical equations that can more accurately predict induced instabilities as well as the growth rate for small amplitude traveling waves. The Floquet analysis here ties the spatial and temporal periodicity of the perturbation to the wavenumber and speed of the traveling wave. An analogous approach of discretizing the governing equations in a moving frame of reference results in LTI system equations that are more appropriate for control synthesis. These system matrix equations predict the same stability characteristics as Floquet analysis, but only the temporal periodicity is handled by the moving frame decomposition. The spatial periodicity is, in essence, handled by the discretization. We show that LQR control, based on the moving frame discretization linear model, can suppress the growing perturbation energy of unstable modes induced by small amplitude traveling waves. The dynamic models used for control are large due to the streamwise coupling of many wavenumbers induced by the upstream traveling wave. A model reduction method for nonlinear input/output systems is developed that will allow

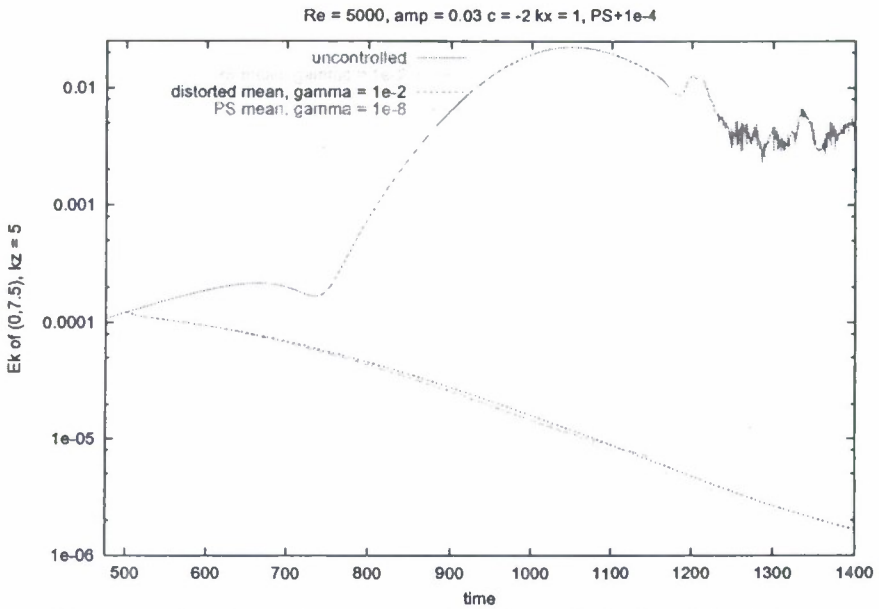

Figure 10: Plot of the log of perturbation energy at the $k_z = 5$ for the distorted mean and Poiseuille mean at Re = 5000 DNS with traveling wave of amplitude 0.03 and upstream speed of 2, with and without LQR.

for efficient controller design.

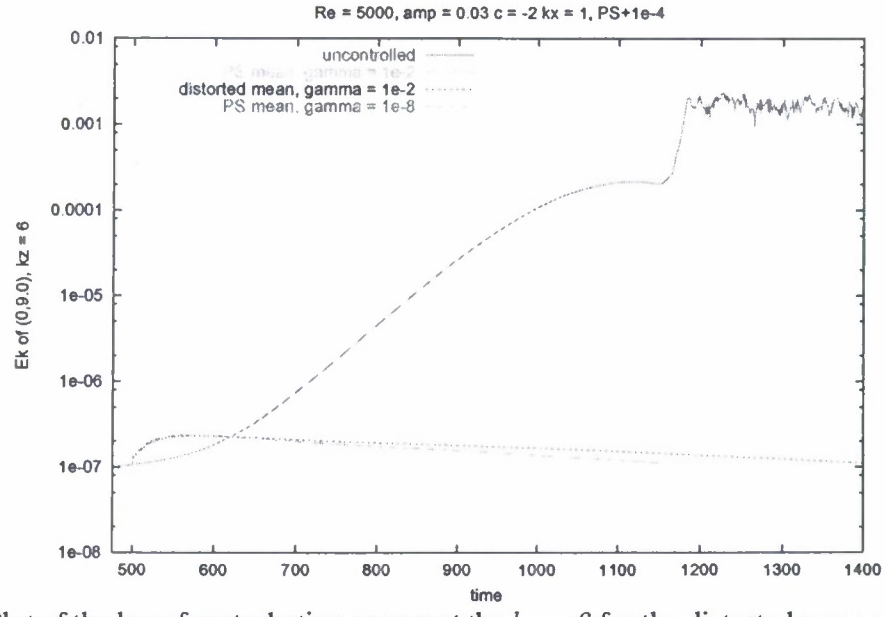

Figure 11: Plot of the log of perturbation energy at the $k_z = 6$ for the distorted mean and Poiseuille mean at Re = 5000 DNS with traveling wave of amplitude 0.03 and upstream speed of 2, with and without LQR.

7 References

[1] S. S. Joshi, J. L. Speyer, and J. Kim, "A systems theory approach to the feedback stabilization of infinitesimal and finite-amplitude disturbances in plane poiseuille flow," *Journal of Fluid Mechanics*, vol. 332, pp. 157–184, 1997.

[2] L. Cortelezzi, K. H. Lee, J. Kim, and J. L. Speyer, "Skin-friction drag reduction via robust reduced-order linear feedback control," *International Journal of Computational Fluid Dynamics*, vol. 11, no. 1-2, pp. 79–92, 1998.

[3] L. Cortelezzi and J. L. Speyer, "Robust reduced-order controller of laminar boundary layer transitions," *Physical Review E*, vol. 58, pp. 1906–1910, August 1998.

[4] K. H. Lee, L. Cortelezzi, J. Kim, and J. L. Speyer, "Application of robust reduced-order controller to turbulent flows for drag reduction," *Physics of Fluids*, vol. 13, no. 5, pp. 1321–1330, 2001.

[5] J. Kim, "Control of turbulent boundary layers," *Physics of Fluids*, vol. 15, pp. 1093–1105, May 2003.

[6] T. Min, S. M. Kang, J. L. Speyer, and J. Kim, "Sustained sub-laminar drag in a fully developed channel flow," *Journal of Fluid Mechanics*, vol. 558, pp. 309–319, 2006.

[7] K. Fukagata, K. Iwamoto, and N. Kasagi, "Contribution of Reynolds stress distribution to the skin friction in wall-bounded flows," *Physics of Fluids*, vol. 14, no. 11, pp. L73–L76, 2002.

[8] K. Fukagata, N. Kasagi, and K. Sugiyama, "Feedback control achieving sublaminar friction drag," in *Proceedings of the 6th Symposium on Smart Control of Turbulence*, (Tokyo, Japan), pp. 143–148, March 6-9 2005.

[9] H. Choi, P. Moin, and J. Kim, "Active turbulence control for drag reduction in wall-bounded flows," *Science*, vol. 262, pp. 75–110, 1994.

[10] R. E. Kelly, "On the stability of an inviscid shear layer which is periodic in space and time," *Journal of Fluid Mechanics*, vol. 27, pp. 657–689, 1967.

[11] J. M. Floryan, "Stability characteristics of wavy walled channel flows," *Physics of Fluids*, vol. 11, Mar. 1999.

[12] S. Selvarajan, E. G. Tulapurkara, and V. Vasanta Ram, "Stability characteristics of wavy walled channel flows," *Physics of Fluids*, vol. 11, Mar. 1999.

[13] A. Or, J. L. Speyer, and H. A. Carlson, "Model reduction of input-output dynamical systems by proper orthogonal decomposition," *AIAA Journal of Guidance, Control, and Dynamics*, vol. 31, no. 2, March-April 2008.

APPENDIX A: Sustained Sub-laminar Drag in a Fully Developed Channel Flow

Published in the *Journal of Fluid Mechanics*, vol. 558, pp. 309-319, 2006.